Journal Pre-proof

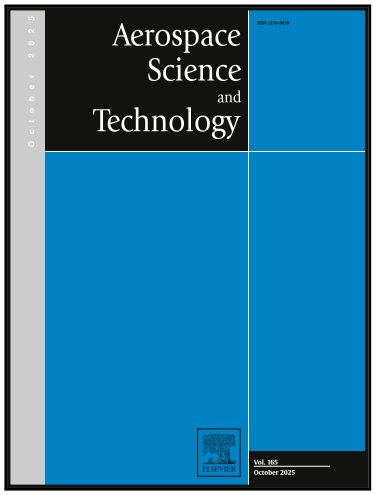

Optimization-Based Task Allocation for Earth Observation in Multi-Satellite Systems

Lorenzo Govoni, Corrado Chiatante, Bjørn Andreas Kristiansen, Tor Arne Johansen, Andrea Cristofaro

PII: S1270-9638(25)01121-6
DOI: https://doi.org/10.1016/j.ast.2025.111058
Reference: AESCTE 111058

To appear in: *Aerospace Science and Technology*

Received date: 10 July 2025
Revised date: 29 September 2025
Accepted date: 7 October 2025

Please cite this article as: Lorenzo Govoni, Corrado Chiatante, Bjørn Andreas Kristiansen, Tor Arne Johansen, Andrea Cristofaro, Optimization-Based Task Allocation for Earth Observation in Multi-Satellite Systems, *Aerospace Science and Technology* (2025), doi: https://doi.org/10.1016/j.ast.2025.111058

Highlights

- Optimization-based Task Allocation for Earth observation in multi-satellite systems
- Hypergraph-based representation to model the satellite capabilities
- Maximization of the coverage of an area of interest
- Minimization of data latency to ground stations

Optimization-Based Task Allocation for Earth Observation in Multi-Satellite Systems*

Lorenzo Govoni[a,*], Corrado Chiatante[b], Bjørn Andreas Kristiansen[c], Tor Arne Johansen[c], Andrea Cristofaro[a]

[a]*DIAG, Department of Computer, Control and Management Engineering, Sapienza University of Rome, Via Ariosto 25, Rome, 00185, Italy*
[b]*Department of Electronic Systems, Norwegian University of Science and Technology (NTNU), Trondheim, 7491, Norway*
[c]*Department of Engineering Cybernetics, Norwegian University of Science and Technology (NTNU), Trondheim, 7491, Norway*

Abstract

The increasing deployment of CubeSats and small satellite constellations for Earth observation has enabled more agile and responsive systems and data services. It has also introduced new challenges related to limited onboard resources, diverse sensor modalities, and the need for dynamic task allocation. Efficient coordination in heterogeneous multi-satellite systems, comprising platforms with differing orbital configurations and imaging capabilities such as optical or radar, requires planning approaches that account for these constraints while minimizing communication overhead and latency. In this paper, we propose a optimization-based task allocation framework that enables heterogeneous, constraint-aware and globally optimal task assignment without relying on inter-satellite communication. Leveraging a hypergraph-based representation to model the compatibility between observation tasks and satellite capabilities, we formulate the allocation problem as a mixed-integer linear program (MILP) that directly incorporates key operational constraints such as energy consumption, data storage, and inter-task timing dependencies. We evaluate the effectiveness of the method using a realistic Earth observation scenario involving the HYPSO-1 and HYPSO-2 hyperspectral CubeSats. Furthermore, we extend the formulation to support secondary objec-

*This research was in part funded by the Research Council of Norway through the grants number 325961 (HYPSCI), 353062 (Agile Operations) and 337495 (SOS).

*Corresponding author
Email address: lorenzo.govoni@uniroma1.it (Lorenzo Govoni)

tives, such as maximizing the coverage of an area of interest and minimizing data latency to ground stations, where our method outperforms baseline heuristics.

Keywords: Earth observation, Task allocation, Multi-agent systems

1. INTRODUCTION

Earth observation remains one of the most significant applications of satellite systems, supporting a wide range of activities such as weather forecasting, disaster management, and environmental monitoring. As a result, imaging satellites now represent a substantial portion of operational space assets [1].

The quality of satellite imagery directly impacts the reliability and effectiveness of the information derived from it [2]. Optical imagers, which rely on sunlight reflected from the Earth's surface, are constrained by atmospheric conditions and diurnal cycles, limiting their availability during cloud cover or nighttime. On the other hand, multispectral and hyperspectral imaging systems have attracted considerable attention due to their ability to capture detailed information across both spatial and spectral domains [3]. These sensors are particularly effective for monitoring dynamic, large-scale phenomena, such as vegetation health, land use change, or water quality, that evolve over time and across extensive geographic areas [4].

In contrast, radar imagers, particularly Synthetic Aperture Radar (SAR), offer observation capabilities independent of weather or lighting conditions [5]. As active sensors they emit microwave signals and measure their reflections, generating high-resolution measurements of surface changes, making them indispensable for detecting events such as landslides, flooding, and wildfires, independent of weather or lighting conditions [5].

Along with the integration of heterogeneous data sources [6], the rapid expansion of satellite constellations and growing user demands with diverse requirements for response and agility, such as emergency responsiveness and coordinated regional surveillance, have intensified the need for autonomous task planning and allocation methods in multi-satellite systems [7]. Satellite constellations have been developed to provide continuous coverage, frequent revisit, and reduced latency [8]. Common design approaches include Walker-type constellations [9], which arrange satellites systematically in orbital planes, streets-of-coverage, emphasizing overlapping swaths for continuous observation, and ground-track-based constellations [10, 11], optimizing repeat coverage over specific regions. The va-

riety and scale of these architectures highlight the increasing importance of autonomous task planning and allocation methods in multi-satellite systems [7].

A common approach for managing this complexity is to decompose the planning process into two subproblems [12]: a high-level task assignment problem, which determines the most appropriate satellite for each observation task, and a lowe-level scheduling problem, which handles the temporal sequencing and resource constraints of each individual satellite. Both levels present significant challenges due to factors such as orbital mechanics, limited onboard resources, downlink bottlenecks, and dynamic observation demands.

On the scheduling side, existing approached can be broadly categorized based on the solution technique employed [13]: exact methods, heuristics, metaheuristics, and machine learning. For instance, [14] introduces a bi-objective optimization model for scheduling active-imaging satellites observing multi-strip ground targets, employing a hybrid approach that combines adaptive large neighborhood search and NSGA-II to balance efficiency and solution quality. A geometric classification-based strategy for optimizing optical acquisitions under stereoscopic and orbital constraints is proposed in [15], targeting periodic sun-synchronous orbits. The work in [16] addresses the increased combinatorial complexity introduced by agile satellites with three degrees of freedom, and explores a range of methods – greedy, dynamic programming, constraint programming, and local search – to solve a simplified observation scheduling problem. Finally, [17] models collaborative task scheduling and attitude planning in attitude space using a novel pseudospectral cooperative genetic algorithm, effectively balancing task coverage and energy efficiency for high-density observation campaigns.

For task allocation, [18] employs an ant colony optimization strategy inspired by natural foraging behavior, assigning tasks based solely on exclusivity, i.e., ensuring each task is assigned to only one satellite. However, this approach omits critical operational constraints during task assignment, handling them only later during per-satellite scheduling. A different strategy is proposed in [12], where task allocation is performed through a centralized-distributed cooperative planning framework. In response to emergency tasks, a master satellite broadcasts observation requests to all subordinate satellites, which then respond with feasibility reports. Based on these responses, the master assigns the task to the most suitable satellite. While this method incorporates satellite capabilities into decision-making, it may suffers from high communication overhead and latency due to the intensive message exchange required.

In the present paper, we aim to overcome these limitations by proposing a unified, optimization-based task allocation framework for heterogeneous multi-

satellite Earth observation missions. Our goal is to enable efficient, constraint-aware task assignment without relying on inter-satellite communication, which introduces delays and complexity in distributed architectures. In this context, heterogeneity arises from the differences in imaging sensor types, such as optical or radar, and from the distinct orbital paths of the satellites. To effectively model the relationship between observation tasks and satellites capabilities, we adopt a hypergraph-based representation, as introduced in [19]. Each observation task, defined by a geographic location and time window, is linked to a corresponding set of feasible satellites through a *Task-to-Satellite mapping*. Our framework incorporates both hardware constraints and operational constraints, including energy consumption, data storage capacity and inter-task timing dependencies, directly into a single mixed-integer linear programming (MILP) formulation [20, 21]. This integration allows for globally optimal task allocation decisions that reflect the capabilities and limitations of each satellite. Furthermore, by executing the optimization on the ground, we eliminate the need for in-orbit message passing, thereby improving responsiveness and simplifying onboard decision-making. We evaluate the effectiveness and applicability of the method in a realistic Earth observation scenario involving the HYPSO-1 and HYPSO-2 CubeSats, which differ in orbit and operate under tight onboard resource limitations. Furthermore, we extend the core formulation to accommodate secondary mission objectives, such as maximizing spatial coverage and minimizing the latency in downlinking data to ground stations. Our simulation results demonstrate that our framework consistently outperforms baseline heuristic methods, including brute-force search and genetic algorithms, especially in complex, multi-objective settings.

The remainder of the paper is organized as follows. Section 2 formulates the problem of target assignment in Earth observation operations involving multi-satellite systems, incorporating application-specific constraints. Section 3 reports simulation results for a representative Earth Observation imaging operations. Section 4 and Section 5 further explore the integration of coverage maximization for an area of interest and the data latency minimization to the ground. Section 6 summarizes the key contributions and proposes future research directions.

Notation: Given a matrix X, we use $X_{i,-}$ to denote its ith row and $X_{-,j}$ to denote its jth column. For a vector $v \in \mathbb{R}^n$, the operator $\mathrm{diag}(v) = M \in \mathbb{R}^{n\times n}$ produces a diagonal matrix M such that $M_{ii} = v_i$ and $M_{ij} = 0$ for all $i \neq j$. Given a matrix X, we denote its Moore–Penrose pseudo-inverse by $X^\dagger$ [22]. The symbol $\mathbb{1}_n$ denotes an n-dimensional column vector of ones.

2. MULTI-SATELLITE EARTH OBSERVATION

In this section, we tackle the Earth observation problem within multi-satellite systems, focusing on determining the optimal assignment of tasks to individual agents to collaboratively accomplish the overall imaging operation. This problem, commonly referred to in literature as *task allocation* [23], involves considering the distinct capabilities of each satellite as well as any constraints associated with task execution.

2.1. Imaging operations

An Earth observation satellite is typically assigned the task of capturing images of a set of targets and communicating them to a corresponding ground station. An observation task, denoted by $\mathcal{T}$, generally comprises n_t independent observation sub-tasks $T_{m,k}$,

$$\mathcal{T} = \{T_{m,k} | m = 1, \ldots, n_t\}, \tag{1}$$

where $k \in \{I, C, S\}$. Specifically, I represents image capturing, C represents communication of the image data, and S represents solar energy harvesting.

We denote the set of available satellites as

$$\mathcal{S} = \{s_i | i = 1, \ldots, n_s\}, \tag{2}$$

where n_s represents the number of satellites involved in the imaging operations. Given the observation task formulation in (1) and the set of satellites $\mathcal{S}$ defined in (2), the task allocation problem can be formally stated as follows.

Problem 1. *Given a set $\mathcal{S}$ of n_s satellites and an observation task $\mathcal{T}$ defined as in* (1) *to be executed, find the optimal sub-task allocation policy $\alpha : \mathcal{T} \to \mathcal{S}$ based on the individual operational constraints of each agent.* •

The mapping in Problem 1 must satisfy both global task allocation specifications and local constraints specific to each agent. This allocation is represented by the *assignment matrix* $\alpha \in \{0, 1\}^{n_s \times n_t}$, where each entry $\alpha_{i,m}$ indicates whether satellite s_i is assigned to sub-task T_m. Moreover, it is assumed that, at any instant of time, each sub-task can be assigned, at most, to one satellite, implying that for each column m, at most one element in $\alpha_{-,m}$ may be non-zero.

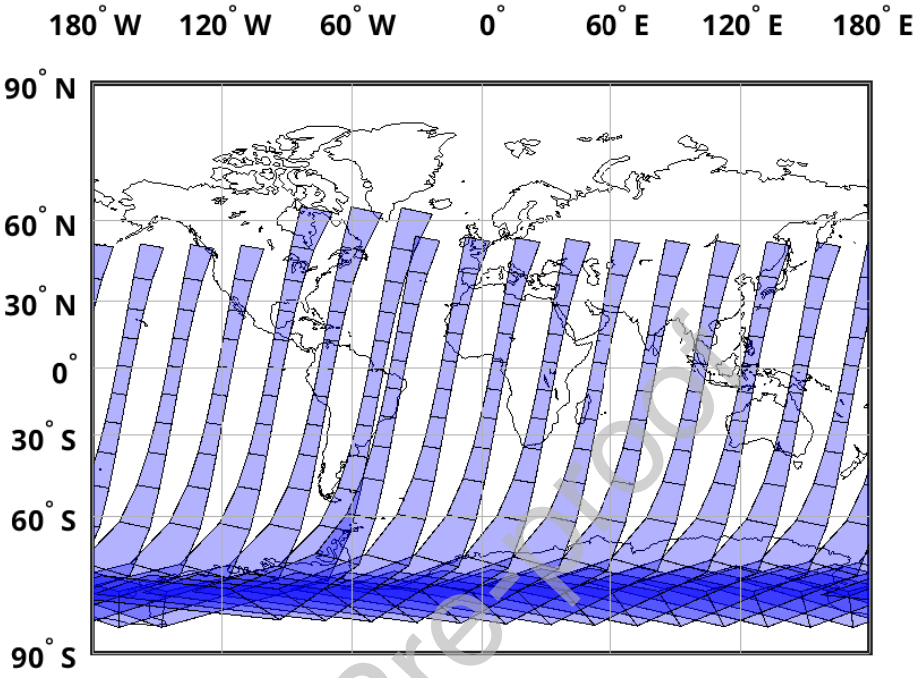

Figure 1: Example of satellite imaging possibilities during one day.

2.2. *Heterogeneity hypergraph*

The solution of Problem 1 critically depends on the orbital dynamics and/or on the type of imaging sensors mounted on each satellite. To capture the heterogeneity inherent in multi-satellite systems, we adopt and adapt the framework proposed in [19, Section III]. Specifically, the authors propose a hypergraph-based representation that models the relationship between the capabilities required to execute a task and the agent's characteristics that enable those capabilities.

In the context of Earth observation, the imaging capacity of a satellite is influenced by factors such as its orbital parameters, allowable off-nadir angles, and the Sun's elevation angle, each of which affects the set of observable targets at a given time. Figure 1 shows an example of orbital propagation, where the blue polygons represent possible imaging field-of-view of a satellite.

Formally, a satellite can execute a sub-tasks $T_{m,k}$, with $k = \{I, C\}$, if it is

at a suitable position, specifically if its attitude $q_b^i(t)$ point towards the position specified by Lon_m and Lat_m at time t_m. Consequently, the heterogeneity of the system can be encoded by a single mapping, referred to as *Task-to-Satellite mapping*. This relationship is defined through a binary matrix $K \in \{0,1\}^{n_s \times n_t}$, where $K_{i,m} = 1$ if and only if satellite i can perform task m, meaning that the ith satellite will be available to point to the target location (Lat_m, Lon_m) at time t_m. Accordingly, for every entry $K_{i,m} \neq 0$ of this mapping we can define a pair $(T_{m,k}, s_i)$ as a feasible assignment, namely s_i is a potential satellite that can execute that task. Each sub-task $T_{m,k}$ can then be defined by a tuple [7], whose elements depend on the particular type k.

- **Imaging sub-task** $T_{m,I}$, represented by the following tuple

$$T_{m,I} =< Lon_m, Lat_m, t_m >, \tag{3}$$

  where (Lon_m, Lat_m) identifies the geographical position of the target to be acquired, t_m represent the time at which satellite s_i passes over the location (Lon_m, Lat_m) [1].

- **Communication sub-task** $T_{m,C}$, represented by the following tuple

$$T_{m,C} =< Lon_m, Lat_m, [t_m^i, t_m^f] > \tag{4}$$

  where the time interval $[t_m^i, t_m^f]$ represents when the satellite s_i is in contact with the ground station located at (Lon_m, Lat_m).

- **Energy sub-task** $T_{m,S}$, represented by the following tuple

$$T_{m,S} =< [t_m^i, t_m^f] >, \tag{5}$$

  where the time interval $[t_m^i, t_m^f]$ represents when the satellite s_i is recharging.

Remark 1. *Given the definition of the energy harvesting task in* (5)*, there is no dependency on orbital position, as all satellites can access the Sun simultaneously. Consequently, in this case, there exists a one-to-one mapping between tasks and satellites.* •

[1] Given the same target position (Lon_m, Lat_m), the same satellite s_i could pass over it more than once if the duration of the campaign is long enough.

In summary, Figure 2 illustrates an example of this heterogeneity hypergraph, considering a general set of n_s satellites and $n_t = 10$ tasks. The dashed arrow represent the link between the two sets, while the edges connecting sub-tasks to the satellites are determined by the specific orbit trajectories of each satellite.

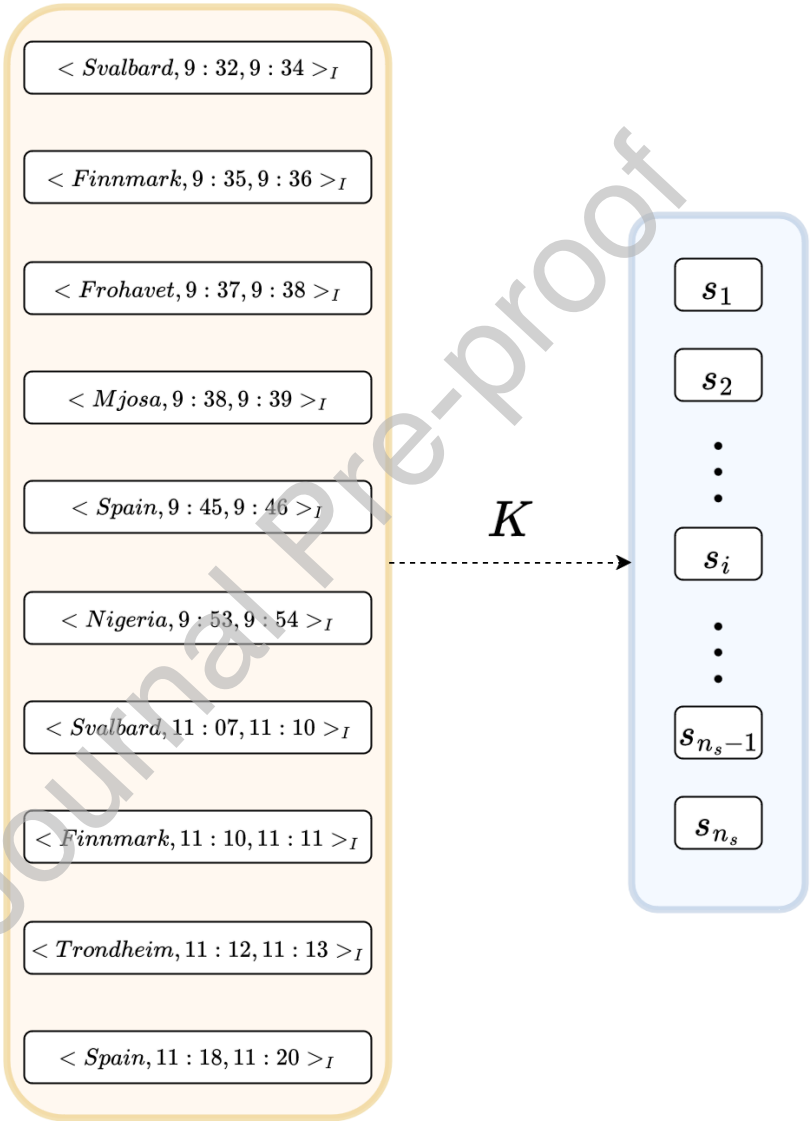

Figure 2: Example of heterogeneity hypergraph.

2.3. Satellite constraints

In multi-satellite applications, several practical constraints related to satellite capabilities must be addresses during an imaging operation. First, for every satellite s_i several operational budgets must be considered, specifically the *data storage capacity* (Bud_{DS_i}) and *energy capacity* (Bud_{S_i}). Given a feasible pair $(T_{m,k}, s_i)$ we define the quantities $Bud_k(s_i)$ and $\delta_k(s_i)$ to encode respectively the amount of data storage occupied and the amount of energy used while performing task $T_{m,k}$.

Remark 2. *The quantities representing budgets and energy costs depend on the specific satellite s_i assigned to the task. This is because, in a heterogeneous system, agents may have different hardware capabilities, leading to varying costs for performing the same action* •

In addition to these budget constraints, each satellite s_i can take two images only if they are at least a time ΔT apart one from each other. As a result, two imaging sub-tasks $T_{m,I}$ and $T_{h,I}$ cannot be simultaneously assigned if their time difference satisfies $|t_m - t_h| < \Delta T$. The absolute value $|\cdot|$ is used since tasks are not inherently ordered, meaning either $t_m > t_h$ or $t_m < t_h$ may hold. Consequently, the task allocation policy must satisfy the following constraints:

- **Data storage constraint**: Given a feasible pair $(T_{m,k}, s_i)$, a satellite s_i incurs a cost when performing a sub-task $T_{m,k}$ with $k = I, C$. Taking an imaging increases the data storage while downlinking the corresponding data decreases it. To capture this effect, we define the function

$$\mathbb{1}_{DS}(K_{i,m}) = \begin{cases} -Bud_C(s_i) & \text{if } k = C \\ Bud_I(s_i) & \text{if } k = I \\ 0 & \text{if } k = S. \end{cases}$$

  where $K_{i,m}$ is the entry of the Task-to-Satellite mapping corresponding to the feasible pair $(T_{m,k}, s_i)$. The data storage constraint is then expressed as:

$$0 \leq \sum_{m=1}^{n_t} \mathbb{1}_{DS}(K_{i,m})\alpha_{i,m} \leq Bud_{DS_i}. \tag{6}$$

  The first inequality encodes the fact that a satellite cannot be assigned to a communication task if it has no images to download to the ground station.

- **Energy constraint**: both imaging and communication sub-tasks consume energy, while solar harvesting sub-task replenishes it. Given the feasible pair $(T_{m,k}, s_i)$, we define the following function to model this effect:

$$\mathbb{1}_S(K_{i,m}) = \begin{cases} -\delta_k(s_i) & \text{if } k = \{C, I\} \\ \delta_S(s_i) & \text{if } k = S. \end{cases}$$

The energy constraint is given by

$$Bud_{S_i} \leq \sum_{m=1}^{n_t} \mathbb{1}_S(K_{i,m})\alpha_{i,m} \leq \overline{Bud_{S_i}}, \tag{7}$$

where Bud_{S_i} and $\overline{Bud_{S_i}}$ correspond respectively to the minimum and maximum energy level of the satellite batteries.

- **Time-mutual exclusion constraint:** Let us define for each satellite s_i a pinning matrix $\Theta^i \in \{0,1\}^{n_i \times n_t}$, with n_i is the maximum amount of images satellite s_i can capture. Its entries are defined as follows

$$\theta^i_{jh} = \theta^i_{jl} = \begin{cases} 1 & \text{if } |t_h - t_l| < \Delta T \\ 0 & \text{otherwise,} \end{cases}$$

valid for all $j = 1, \ldots, n_i$ and for all $h, l = 1, \ldots, n_t$ and $h \neq l$. Consequently, the time-mutual exclusion constraint for each satellite s_i can be defined as follows

$$\Theta^i \alpha^T_{i,-} = 1, \tag{8}$$

2.4. Optimization problem

In this section, we revisit the Mixed Integer Linear Programming (MILP) formulation originally proposed in [19], adapting it to the context of the multi-satellite task allocation problem defined in Problem 1. Incorporating the operational and hardware constraints outlined in (6)–(8), the resulting MILP formulation is expressed as follows.

$$\underset{\alpha}{\text{minimize}} \quad \sum_{m=1}^{n_t} ||\Xi_m \alpha_{-,m}||^2 \tag{9a}$$

$$\text{subject to} \quad \mathbb{1}_{n_s}^T \alpha_{-,m} \leq 1 \tag{9b}$$

$$0 \leq \sum_{m=1}^{n_t} \mathbb{1}_{DS}(K_{i,m}) \alpha_{i,m} \leq Bud_{DS_i} \tag{9c}$$

$$Bud_{S_i} \leq \sum_{m=1}^{n_t} \mathbb{1}_{S}(K_{i,m}) \alpha_{i,m} \leq \overline{Bud_{S_i}} \tag{9d}$$

$$\Theta^i \alpha_{i,-}^T = 1 \tag{9e}$$

$$n_{i,m,min} \leq \mathbb{1}_{n_t}^T \alpha_{i,-}^T \leq n_{i,m,max} \tag{9f}$$

$$\alpha \in \{0,1\}^{n_s \times n_t}, \tag{9g}$$

where all the constraints must be satisfied for every $i = \{1, \ldots, n_s\}$ and for every $m = \{1, \ldots, n_t\}$.

- In the cost function (9a), the matrix $\Xi_m = I_{n_s} - S_m S_m^\dagger$ is used to penalize infeasible task allocations. Here, the matrix $S_m = \text{diag}(K_{-,m})$ represents the specialization matrix associated with sub-task $T_{m,k}$, where K is the Task-to-Satellite mapping defined in Section 2.2. The diagonal entries of S_m reflect whether each satellite is capable of executing task m; specifically, a zero entry in position (i, i) indicates that satellite i lacks the necessary capabilities. Consequently, the matrix Ξ_m assigns a higher cost in (9a) when a task is allocated to an incompatible satellite, thereby enforcing capability-aware allocation decisions.
- The constraint (9b) imposes that each sub-task can be perform by at most one satellite.
- The constraint (9f) enables the imposition of a minimum and a maximum number of tasks for the satellite s_i. The minimum number of agents required by each task must be at least one, while regarding the maximum number of agents the parameters must satisfy the following condition

$$\sum_{i=1}^{n_s} n_{i,m,max} \leq n_t.$$

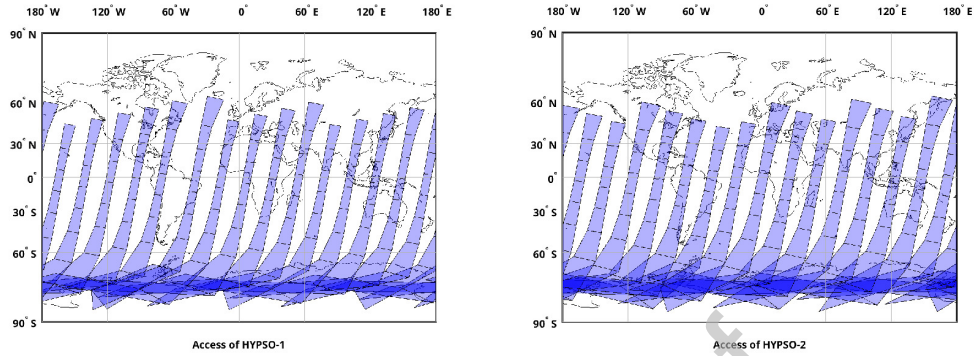

Figure 3: Satellite access for HYPSO-1 and HYPSO-2.

In addition, the formulation (9) enables the inclusion of a weight matrix that multiplies the assignment matrix α, allowing task prioritization to be explicitly encoded. However, for the remainder of the paper, we assume all tasks have equal priority.

3. SIMULATION: EARTH OBSERVATION

In this section, we address the task allocation in a multi-satellite system where the set $\mathcal{S}$, defined in (2), is composed of two satellites with pushbroom hyperspectral imagers, HYPSO-1 [24] and HYPSO-2 [25], during Earth observation nominal operations. The constellation is requested to cover a set of targets scattered over the entire Earth's surface.

Remark 3. *Due to differences in communication capabilities, satellites HYPSO-1 and HYPSO-2 can perform approximately 5 and 40 raw image downlinks per day, respectively [25]. This significant disparity could result in a trivial task allocation problem, where one satellite dominates the execution of sub-tasks. To avoid this and enable a more balanced and meaningful analysis, we assume in this paper that both satellites have comparable imaging capabilities and can deliver a similar number of images. This will be the case e.g. if HYPSO-1 compresses or processes images more than HYPSO-2.* •

3.1. Simulation set-up

In this simulation, we consider a one-day observation campaign spanning from *03-Dec-2024 13:20:00* to *04-Dec-2024 13:20:00*. Figure 3 reports the orbital

propagation over the observation period of HYPSO-1 and HYPSO-2 on the left and on the right, respectively. Orbit propagation in all simulation cases was performed through the Python library Skyfield [26], with the Simplified General Perturbations model 4 (SGP4) propagator using Two-Line Elements (TLEs) as initial conditions. SGP4 is a semi-analytic model consistent with the TLE format and includes the principal perturbations typically embedded in TLEs [2].

The blue polygon represent the field-of-view of each satellite, where the time mutual exclusion interval in (8) is set to $\Delta T = 5$ min. The area available to the satellites for imaging further depends on the orbital altitude, the off-nadir angle, and the Sun-elevation angle. The maximum off-nadir angle was set to 40 degrees, as the spatial resolution degrades and atmospheric effects degrade images more at higher values, both leading to low image quality. Similarly, a minimum Sun elevation angle has been set to 10 degrees to allow only sunlit areas to be imaged. This explains the absence of blue polygons in the northern regions in Figure 3, where, during winter, sunlight is unavailable or have very low elevation angles.

The observation sub-tasks considered in the simulation are listed in Table 1, comprising a total of $n_t = 158$ sub-tasks. Each sub-task $T_{m,k}$, with $k \in \{I, C, S\}$, is divided among the two different satellites.

	$T_{m,I}$	$T_{m,C}$	$T_{m,S}$
HYPSO-1	24	15	42
HYPSO-2	20	15	42

Table 1: Number of potential sub-tasks for each satellite. Tasks are divided into imaging ($T_{m,I}$), communication ($T_{m,C}$), and energy storage ($T_{m,S}$).

The imaging targets were randomly selected on the map and are depicted in Figure 4a. The communication tasks, shown in Figure 4b, correspond to the locations where either HYPSO-1 or HYPSO-2 establishes contact with the ground station in Svalbard. The energy sub-tasks where uniformly selected within the observation time window.

The time dependency of imaging and communication tasks is visually illustrated using a color-coded legend, defined by the color bar adjacent to the plot. Tasks are arranged sequentially, from the earliest to the latest execution time.

[2] It should be noted that SGP4 is not a high-fidelity numerical integrator: it does not include a high-degree geopotential, detailed atmospheric density models, or explicit SRP and high-accuracy third-body models beyond the approximations inherent in the SGP4 formulation. Consequently, SGP4 is appropriate for short-to-medium term propagation consistent with TLE accuracy.

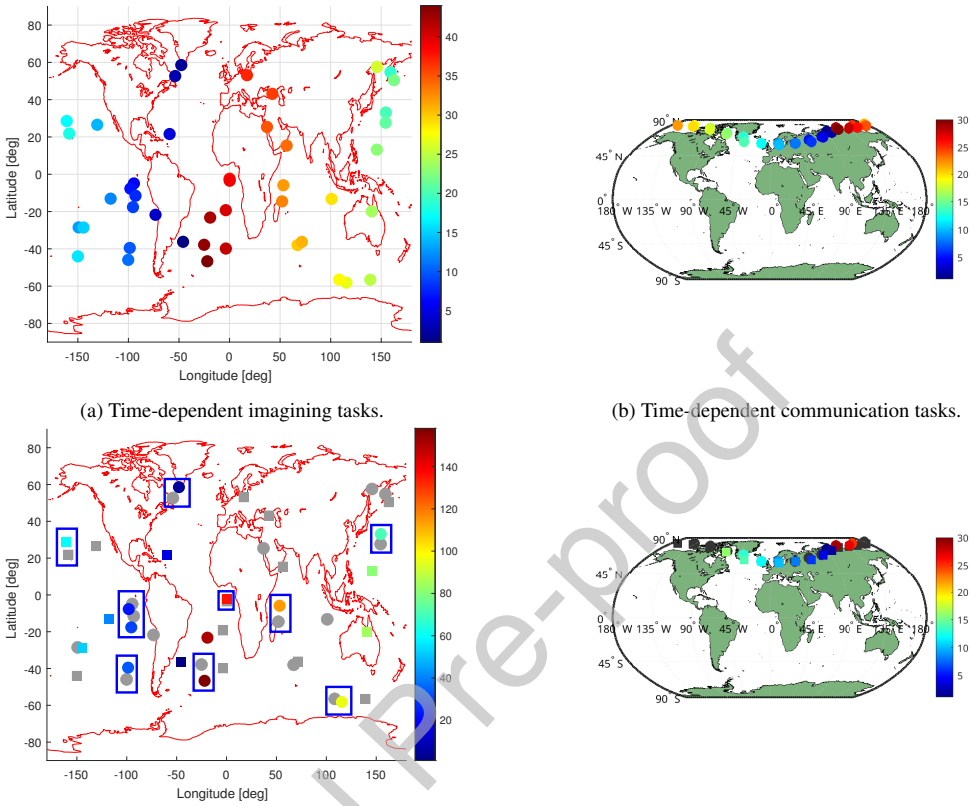

(a) Time-dependent imagining tasks.

(b) Time-dependent communication tasks.

(c) Assigned imagining tasks.

(d) Assigned communication tasks.

Figure 4: Imaging and communication tasks. The color-coded legend, adjacent to the plot, encodes the time dependency of the tasks, which are arranged sequentially, from the earliest to the latest execution time. The grey dots and squares in (c) and (d) represent the unassigned tasks. The blue rectangles highlight imaging tasks that occur within a 5-minute interval of each other. Due to constraint (9e), such tasks cannot be assigned simultaneously.

Regarding the data storage constraint in (9c), we have assumed that capturing an image and transmitting it to the ground station have the same storage cost. Consequently, the data storage budget Bud_{DS_i} is considered as the maximum number of pictures each satellite can store at the end of the observation campaign. For this simulation, HYPSO-1 is limited to storing a maximum of 5 images, while HYPSO-2 can store up to 10 images.

	$T_{m,I}$		$T_{m,C}$		$T_{m,S}$	
	Ass.	Unass.	Ass.	Unass.	Ass.	Unass.
HYPSO-1	9	15	5	10	11	31
HYPSO-2	8	12	6	9	11	31

Table 2: Number of assigned and unassigned sub-tasks for each satellite. Tasks are divided into imaging ($T_{m,I}$), communication ($T_{m,C}$), and energy storage ($T_{m,S}$). The unassigned tasks result from budget and time constraints.

3.2. Simulation results

In this section, we present the resolution of the task allocation problem defined in (9). Figure 4c illustrates the imaging tasks assigned to the two satellites, HYPSO-1 and HYPSO-2, while Figure 4d displays the assigned communication tasks. The same color-coded legend as in Figure 4 is used for consistency. In Figure 4c, the dots represent the 8 imaging tasks assigned to HYPSO-1, while the squares denote the 9 images allocated to HYPSO-2. Following the same notation, for the communication tasks, HYPSO-1 is assigned to 7 tasks, while HYPSO-2 is assigned to 8 task. At the end of the observation campaign, both HYPSO-1 and HYPSO-2 have one image stored, pending communication.

Unassigned tasks are represented as gray dots and squares in Figure 4c and Figure 4d. These tasks were excluded due to either the budget constraint (9c) or the time-mutual exclusion constraint (9e) or both. Specifically, in Figure 4c, the blue rectangles highlight imaging tasks that occur within a 5-minute interval of each other. Due to constraint (9e), such tasks cannot be assigned simultaneously.

Table 2 summarizes the number of assigned and unassigned sub-tasks for each satellite, categorized into imaging ($T_{m,I}$), communication ($T_{m,C}$), and energy storage ($T_{m,S}$) tasks. Notably, all energy storage tasks were successfully assigned to both satellites, satisfying the energy constraint defined in (9d).

4. MAXIMIZATION OF SPATIAL COVERAGE

In this section, we formulate the problem of optimally covering an area of interest $\mathcal{A}$ given a set of target locations $\mathcal{P}$. This is approached within the task allocation formalism, using the same satellite set $\mathcal{S}$ used in Section 3. The set $\mathcal{P}$ is defined as follows

$$\mathcal{P} = \{p_h =< Lon_h, Lat_h > | h = 1, \ldots, n_p\} \subset \mathcal{A} \tag{10}$$

where n_p represents the number of targets considered in the coverage problem. However, maximizing the coverage of $\mathcal{A}$ may lead to a reduction of the quality of the acquired images. Therefore, the objective is to jointly maximize both the spatial coverage of $\mathcal{A}$ and the resolution of the assigned images. The resolution of each capture is computed based on the specifications of the optical imager and the orbital parameters. For simplicity, this analysis focuses on the cross-track resolution, as it is more significantly affected by off-nadir angles compared to the along-track resolution.

The formal definition of the problem is summarized in the following statement.

Problem 2. *Given a team of n_s satellites, an area of interest $\mathcal{A}$ and a set of n_p target locations $\mathcal{P}$ defined in* (10)*, determine the optimal allocation of the target points to satellites in order to maximize both the coverage of $\mathcal{A}$ and the resolution of the captured images, while satisfying the operational constraints.* •

Satellite image resolution can differ at nadir and off-nadir. For Hyperspectral imagers, the spatial resolution [27] at nadir can be calculated as :

$$\text{Resolution}_{\text{nadir}} = \frac{H \cdot h_{\text{slit}}}{f \cdot N_{\text{pixels}}} \tag{11}$$

where:

- H is the orbital altitude of the satellite,
- h_{slit} is the slit height,
- f is the focal length of the optical system,
- N_{pixels} is the number of detector pixels along the cross-track dimension,

When accounting for off-nadir imaging (with θ being the off-nadir angle), the ground resolution deteriorates because of geometric effects. Assuming small angular displacements between successive pixels [28], the following formula can be used to approximate the off-nadir resolution:

$$\text{Resolution}_{\text{off-nadir}} = \frac{\text{Resolution}_{\text{nadir}}}{\cos^2(\theta)} \tag{12}$$

For each target $p_h \in \mathcal{P}$ we define a corresponding imaging sub-task $T_{m,I}$. In the context of the coverage problem, the imaging sub-task representation defined in (3) is extended with an additional parameter: $poly_m$: the footprint of the image taken by satellite s_i at time t_m, centered in (Lon_m, Lat_m). The augmented imaging sub-task representation is thus given by

$$T_{m,I} =< Lon_m, Lat_m, t_m, poly_m > \tag{13}$$

Moreover, to each footprint $poly_m$ we define the off-nadir resolution $\rho_m \in \mathbb{R}$, based on the formula in (12), to quantify the image resolution degradation as the imaging direction deviates from nadir.

The estimation of the footprint generation for each target is represented in Figure 5. From a satellite and target pair, the mission planning pipeline computes the maximum elevation point over the target [25]. At this instant of time, the simulator provides both the timestamp and the quaternion required to orient the satellite imager to the selected target, expressed in body-frame (x_B, y_B, z_B). The footprint polygon $poly_m$ is then generated by considering the number of frames captured along the satellite's ground track, the imager's frame-rate, and the field of view of the payload. It is generated by tracing field-of-view rays to their Earth intersections and extracting the boundary coordinates. HYPSO-1 and HYPSO 2 share the same amount of frames in nominal imaging operations - 598 frames. However, choosing different frame rates (8 FPS for HYPSO-1 and 12 FPS for HYPSO-2) leads to longer images for HYPSO-2 as the payload captures frames for a longer time.

4.1. Optimization Problem

To address Problem 2, we extend the optimization problem (9) by introducing two additional cost terms: one to account for the total covered area within $\mathcal{A}$ and another to maximize the overall resolution of the assigned imaging tasks.

When capturing images over a set of target locations p_h within $\mathcal{A}$, some images may overlap. To prevent double-counting these regions in the cost function, we introduce an overlap matrix $O \in \mathbb{R}^{n_t \times n_t}$ to encode possible overlapping among the polygons. The elements $o_{i,j}$ of this matrix are defined as follows

$$o_{i,j} = \begin{cases} 1 & \text{if } poly_i \cap poly_j \neq \emptyset \\ 0 & \text{otherwise.} \end{cases} \tag{14}$$

To ensure that the overlapping areas are subtracted only when both overlapping polygons are assigned, we define a binary decision variable $z \in \{0,1\}^{n_t \times n_t}$. This

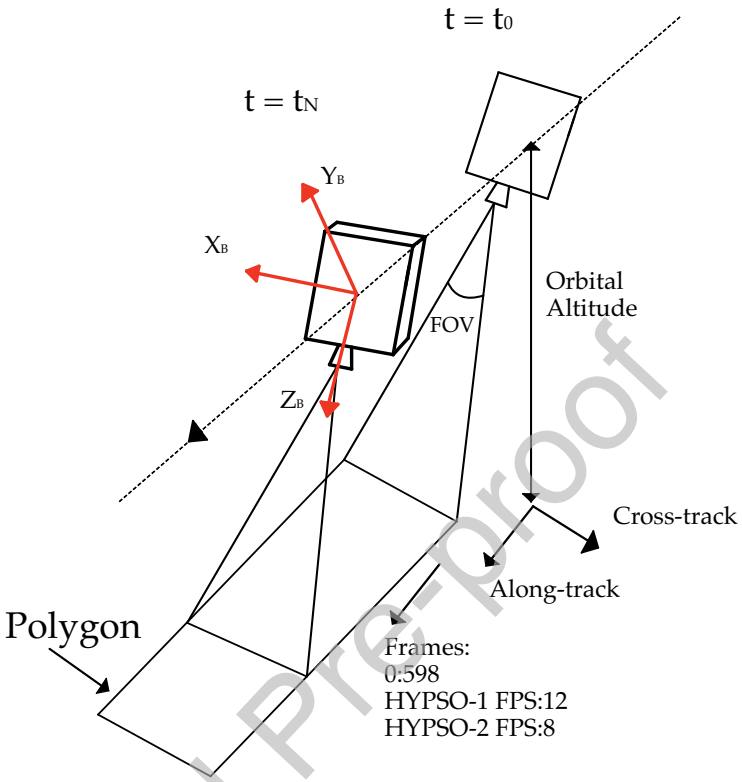

Figure 5: Imaging scanning mode for HYPSO-1 and HYPSO-2. The polygonal imaging areas are a direct result of the pushbroom imaging functionality used in the scanning modes.

variable encodes whether two overlapping polygons are simultaneously assigned in the coverage problem. To relate the matrix α with z, we consider the following logical expression

$$\alpha_{m,i} \wedge \alpha_{m,j} \rightarrow z_{i,j}, \tag{15}$$

valid for all the non-zero entries of matrix O and for all $m \in \{1, \ldots, n_t\}$. This logical condition is translated into the following binary linear constraint [29]

$$z_{i,j} \geq \alpha_{m,i} + \alpha_{m,j} - 1 \quad \forall m = \{1, \ldots, n_t\}. \tag{16}$$

Let us define $\mathrm{Area}(\cdot)$ as the operator that returns the area of a given set. Thus, the

resulting cost function is given by

$$\begin{aligned}\mathcal{J}(\alpha, z, \mathcal{A}, \mathcal{P}) = &\sum_{i=1}^{n_s}\sum_{m=1}^{n_t} \alpha_{i,m}\,\text{Area}(poly_m \cap \mathcal{A}) \\ &- \sum_{i=1}^{n_t}\sum_{i=j}^{n_t} o_{i,j} z_{i,j}\,\text{Area}\left((poly_i \cap poly_m) \cap \mathcal{A}\right).\end{aligned} \tag{17}$$

On the other hand, to account for the maximization of the overall resolution of the assigned pictures, we introduce the following resolution-based cost function

$$\mathcal{R}(\alpha) = \frac{1}{N}\sum_{i=1}^{n_s}\sum_{m=1}^{n_t} \rho_m \alpha_{i,m}, \tag{18}$$

where N is the total number of picture taken and ρ_m represents the resolution associated with each image introduced in (13).

Since a satellite may pass over the same target location multiple times within a given time window, we impose a constraint to ensure that each target is assigned only once. We define a binary matrix $\Gamma \in \{0,1\}^{n_p \times n_t}$, where $\Gamma_{h,m} = 1$ if $(Lon_m, Lat_m) \equiv (Lon_h, Lat_h)$. Consequently, the *location-mutual exclusion* constraint is defined as follows

$$\sum_{h=1}^{n_p} \Gamma_{h,-}\alpha_{i,-}^T = 1 \quad \forall i \in \{1, \ldots, n_s\}. \tag{19}$$

The resulting formulation for the task allocation in the coverage problem is given by

$$\min_{\alpha,z} \; c\sum_{m=1}^{n_t} ||\Xi_m \alpha_{-,m}||^2 - \ell\mathcal{J}(\alpha, z, \mathcal{A}, \mathcal{P}) - k\mathcal{R}(\alpha) \tag{20a}$$

$$\text{s.t. } \mathbb{1}_{n_s}^T \alpha_{-,m} \leq 1 \tag{20b}$$

$$0 \leq \sum_{m=1}^{n_t} \mathbb{1}_{DS}(K_{i,m})\alpha_{i,m} \leq Bud_{DS_i} \tag{20c}$$

$$Bud_{S_i} \leq \sum_{m=1}^{n_t} \mathbb{1}_{S}(K_{i,m})\alpha_{i,m} \leq \overline{Bud_{S_i}} \tag{20d}$$

$$\Theta^i \alpha_{i,-}^T = 1 \tag{20e}$$

$$\sum_{h=1}^{n_p} \Gamma_{h,-}\alpha_{i,-}^T = 1 \tag{20f}$$

$$n_{s,m,min} \leq \mathbb{1}_{n_t}^T \alpha_{i,-}^T \leq n_{s,m,max} \tag{20g}$$

$$\alpha \in \{0,1\}^{n_s \times n_t}, \tag{20h}$$

where the constraints must be satisfied for every $i = \{1, \ldots, n_s\}$ and for every $m = \{1, \ldots, n_t\}$. In the cost function (20a), the positive tuning parameters c, ℓ and k are selected such that $c \gg \ell$ and $c \gg k$, meaning that the penalization of bad allocations in the first term is preferred to the maximization of the coverage. The trade-off between coverage and resolution is governed by the ratio ℓ/k. A higher ratio prioritizes coverage, while a lower ratio emphasizes high-resolution imaging.

4.2. Simulation results

In this section, we present the simulation results for solving the coverage optimization problem defined in Problem 2. The simulation is based on a one-day observation campaign, spanning from *07-Feb-2025 10:35:23* to *08-feb-2025 11:17:43*, aimed at covering an area around Frohavet. The satellite set $\mathcal{S}$, is the same used in Section 3 composed of HYPSO-1 and HYPSO-2.

Figure 6a illustrates the area of interest $\mathcal{A}$, which is delineated by a purple polygon, while the target locations p_h are depicted with red dots. Figure 6b reports all the possible polygons that can be assigned for the coverage task. The polygons corresponding to HYPSO-1 are shown in blue, while those corresponding to HYPSO-2 are depicted in green. It is noteworthy that several polygons overlap, and each target location is visited at least twice by each satellite. Thus,

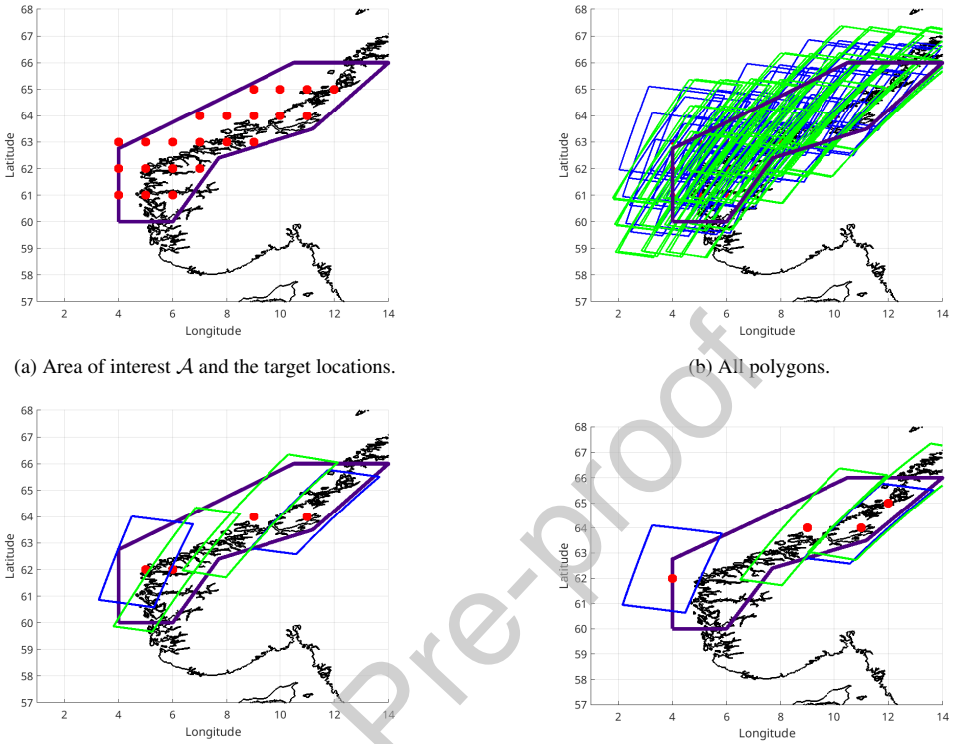

(a) Area of interest $\mathcal{A}$ and the target locations.

(b) All polygons.

(c) Assigned polygons: $\ell \gg k$.

(d) Assigned polygons: $\ell \ll k$.

Figure 6: Coverage simulation. The polygons corresponding to HYPSO-1 are shown in blue, while those corresponding to HYPSO-2 are depicted in green.

the constraint (20f) and the introduction of the decision variable z, play a key role in maximizing the area coverage by limiting the overlap.

Figure 6c and Figure 6d show trade-off between coverage and resolution under different optimization priorities. Specifically, Figure 6c illustrates the task assignment when the objective is to maximize coverage, obtaining a coverage of 88.95% of the desired area $\mathcal{A}$, with a mean spatial resolution of 74.83 m. On the other hand, Figure 6d reports the allocation when prioritizing high-resolution imaging. In this scenario, the selection of higher-quality comes at the expense of reduced coverage, resulting in 62.06% of $\mathcal{A}$, while the mean spatial resolution improves to 79.22 m.

4.3. Computational time

In this section, we analyze the computational time required for solving the optimization problem (20) under the objective of maximizing the coverage of the area $\mathcal{A}$, i.e., when the weighting factors are chosen such that $\ell \gg k$.

All simulations were conducted on a laptop equipped with a 13th Gen Intel(R) Core(TM) i7-13620H CPU (10 cores, 16 threads, 2.40 GHz base clock), 16GB LPDDR5-4800 RAM, running Ubuntu 24.04.

To asses efficiency of the proposed optimization approach, we compare its performance against two well-known approaches: *brute force*, which evaluates all the possible assignments to find the optimal one, and *genetic algorithm*, a metaheuristic approach that iteratively improves the solution through selection, crossover and mutation [30]. All the computations were carried out in Python and the optimization problem (20) is solved using the Gurobi Optimizer [31].

The comparison is based on three key performance metrics:

- **Mean Solving Time** (MST): the average time required to find a solution.
- **Standard Deviation for Solving Time** (SDST): measures the variability in solving time.
- **Solution Quality**: the percentage of the area $\mathcal{A}$ successfully covered by the assigned polygons.

Table 3 summarizes the computational results. Since the genetic algorithm is stochastic approach, we ran it 30 times to and the data reported in Table 3 represent the average performance over these executions.

Algorithm	**MST (s)**	**SDST (s)**	**Solution Quality**
Brute Force	64.30	0	88.95%
Genetic Algorithm	35.78	5.05	88.57%
Optimization	0.76	0	88.95%

Table 3: Comparison of Task Allocation Algorithms.

The brute force approach, while guaranteeing an optimal solution, exhibits an exponential increase in computational time, making it impractical for large-scale problems. The genetic algorithm provides a near-optimal solution with a significant reduction in computational time. The standard deviation of 5.05 s indicates variability in convergence times due to the stochastic nature of the approach.

The proposed approach with the Gurobi optimizer significantly outperforms both methods in terms of speed, solving the problem in under a second (0.76 s) while maintaining the same (global) optimal solution as brute force.

5. MINIMIZATION OF DATA LATENCY TO THE GROUND

In this section, we consider the problem of assigning observation sub-tasks $T_{m,k}$ while minimizing the data latency to the ground, defined as the time from image capture until it is available in a ground station.

5.1. Optimization problem

To address this problem, we extend the imaging sub-tasks $T_{m,I}$ defined in (3), by introducing an additional property $\sigma_m \in \mathbb{R}$, which encodes the data latency of satellite s_i. Specifically, the data latency can be defined as:

$$\sigma_m = T_{\text{travel}}(s_i, Lon_m, Lat_m) + T_{\text{transmit}}(s_i, C_i), \tag{21}$$

where the two components are defined as follows:

- *Travel time* $T_{\text{travel}}(s_i, Lon_m, Lat_m)$: correspond to the satellite's travel time along its orbit from the image acquisition was made to the start of the next communication window. It primarily depends on the relative positions of the imaging location and the ground stations.
- *Transmission time* $T_{\text{transmit}}(s_i, C_i)$: is the time required to transmit the data to the ground station as well as orbital parameters and it depends on the communication capabilities C_i of the satellite s_i. It can be either considered constant (depending only on image data size) or modeled as a function of the communication quality.

The new sub-task formulation is the following

$$T_{m,I} =< Lon_m, Lat_m, t_m, \sigma_m > . \tag{22}$$

Minimizing data latency is meaningful only if the allocation policy ensures that, whenever an imaging task is assigned, the temporally nearest feasible communication task is also selected. However, this requirement may conflict with constraint (9e), potentially rendering the problem infeasible. To enforce this coupling, we introduce the following linear soft constraint

$$\Gamma^i \alpha_{i,-}^T = \varepsilon_i, \quad \forall i = \{1, \ldots, n_s\}, \tag{23}$$

where the matrix Γ^i is constructed such that the constraint enforces $\alpha_{i,j} \Leftrightarrow \alpha_{i,h}$, where j indexes an imaging task $T_{j,I}$ and h the nearest subsequent communication task $T_{h,C}$ in time for satellite s_i. This ensures that assigning an imaging task implies assigning its corresponding communication task, and vice versa. On the other hand, the slack variable ε_i relaxes the constraint by allowing necessary violations to be penalized in the objective function.

To account for the minimization of the data latency, we define the following cost function

$$\mathcal{D}(\alpha) = \sum_{i=0}^{n_s} \sum_{m=0}^{n_t} \alpha_{i,m} \sigma_m. \tag{24}$$

The resulting optimization task allocation problem reads as

$$\begin{aligned}
\underset{\alpha}{\text{minimize}} \quad & \sum_{m=1}^{n_t} c||\Xi_m \alpha_{-,m}||^2 + \hbar \mathcal{D}(\alpha) + \lambda \sum_{i}^{n_s} \varepsilon_i && \text{(25a)}\\
\text{subject to} \quad & \mathbb{1}_{n_s}^T \alpha_{-,m} \leq 1 && \text{(25b)}\\
& 0 \leq \sum_{m=1}^{n_t} \mathbb{1}_{DS}(K_{i,m}) \alpha_{i,m} \leq Bud_{DS_i} && \text{(25c)}\\
& Bud_{S_i} \leq \sum_{m=1}^{n_t} \mathbb{1}_{S}(K_{i,m}) \alpha_{i,m} \leq \overline{Bud_{S_i}} && \text{(25d)}\\
& \Theta^i \alpha_{i,-}^T = 1 && \text{(25e)}\\
& \Gamma^i \alpha_{i,-}^T = \varepsilon_i && \text{(25f)}\\
& \varepsilon_i \geq 0 && \text{(25g)}\\
& n_{s,m,min} \leq \mathbb{1}_{n_t}^T \alpha_{i,-}^T \leq n_{s,m,max} && \text{(25h)}\\
& \alpha \in \{0,1\}^{n_s \times n_t}, && \text{(25i)}
\end{aligned}$$

where the constraints must be satisfied for every $i = \{1, \ldots, n_s\}$ and for every $m = \{1, \ldots, n_t\}$. In the cost function (25a), the positive tuning parameters c, h and λ are selected such that $c \gg h$ and $c \gg \lambda$. This ensures that task allocation quality is prioritized over latency minimization.

5.2. Simulation results

In this section, we report the simulation results, showing the impact of the minimization of the data latency on the task allocation. Specifically, in equation (21) we assume the time required to transmit the data to the ground T_{transmit} constant.

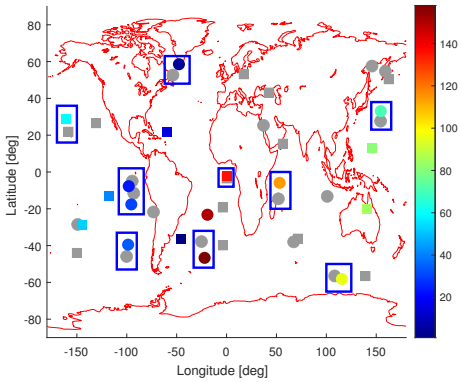

(a) Earth observation: assigned imagining tasks.

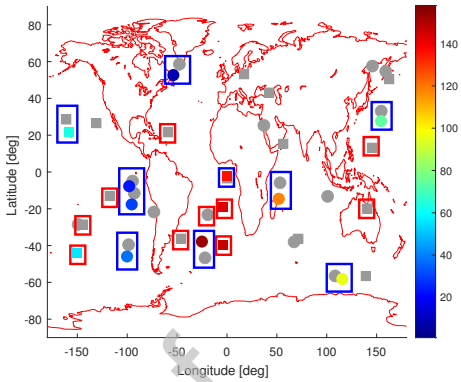

(b) Data latency minimization: assigned imaging tasks.

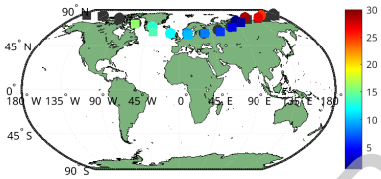

(c) Earth observation: assigned communication tasks.

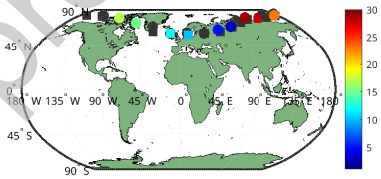

(d) Data latency minimization: assigned communication tasks.

Figure 7: Comparison between the solution of problem (9) and problem (25). The color-coded legend, adjacent to the plot, encodes the time dependency of the tasks, which are arranged sequentially, from the earliest to the latest execution time. The grey dots and squares in (a) and (b) represent the unassigned tasks. The red squares highlight the differences in the allocation policy between problem (9) and problem (25).

We consider the same simulation set-up defined in Section 3 focusing the attention on the assignment of the imaging tasks.

Table 4 reports the outcomes of solving the optimization problem (9), which does not account for the data latency, and the optimization problem (25), which incorporates the extra cost term (24) to explicitly minimize the data latency. As shown in the third column for each case, introducing this cost term significantly reduces the overall data latency, while assigning the imaging and communication tasks.

Figure 7 compares the assigned tasks, both imaging and communication, ob-

	Problem (9)			Problem (25)		
	$T_{m,I}$	$T_{m,C}$	σ_m [min]	$T_{m,I}$	$T_{m,C}$	σ_m [min]
HYPSO-1	9	5	568	8	6	501
HYPSO-2	8	6	521	5	3	314

Table 4: Comparison of total data latency resulting from the solutions to Problem (9) and Problem (25).

tained by both optimization problems. The inclusion of the data latency cost term in problem (25) leads to a noticeable shift in the task allocation strategy. While data latency is clearly reduced, as shown in Table 4, this improvement comes at the cost of assigning fewer tasks to the satellites overall. Specifically, we have a change in the assignment of the communication tasks, which are now near in time to the assigned imaging tasks. The red rectangles in Figure 7b highlight the assigned imaging tasks that differ from the solution of (9).

Remark 4. *The results in Table 4 show that, for both optimization problems* (9) *and* (25)*, not all images are downlinked, leading to additional data latency not captured in* (21)*. However, the addition of the extra cost term* (24) *implicitly reduces on-board image storage. Specifically, with problem* (25)*, HYPSO-1 keeps only 2 images instead of 4, while HYPSO-2 stores the same number as in* (9)*.* •

6. CONCLUSION

In this paper, we present a mixed-integer linear programming approach to address the task allocation problem in heterogeneous satellite constellations while accounting for key operational constraints. The proposed method incorporates mission-specific requirements, such as data storage capacity, energy budgets and inter-task timing constraints, to enable efficient planning fro hyperspectral Earth observation missions. We validated our method through numerical simulations involving the HYPSO-1 and HYPSO-2 CubeSats, incorporating secondary optimization objectives such as maximizing coverage and minimizing data latency to the ground stations. The results demonstrate the flexibility of the framework across various operational scenarios and show a significant reduction in the computational burden compared to baseline heuristics like brute force search and genetic algorithm. Future works will be devoted to extend the proposed framework to a decentralized setting by leveraging inter-satellite communication, as well as incorporating additional dynamical agents beyond satellites into the task allocation formalism.

Declaration of interests

The authors declare the following financial interests/personal relationships which may be considered as potential competing interests:

Corrado Chiatante reports financial support was provided by Research Council of Norway. Bjorn Andreas Kristiansen reports financial support was provided by Research Council of Norway. Tor Arne Johansen reports financial support was provided by Research Council of Norway. If there are other authors, they declare that they have no known competing financial interests or personal relationships that could have appeared to influence the work reported in this paper.

References

[1] Q. Zhao, L. Yu, Z. Du, D. Peng, P. Hao, Y. Zhang, P. Gong, An overview of the applications of earth observation satellite data: impacts and future trends, Remote Sensing 14 (8) (2022) 1863.

[2] S. Agrawal, G. Khairnar, A comparative assessment of remote sensing imaging techniques: Optical, sar and lidar, The International Archives of the Photogrammetry, Remote Sensing and Spatial Information Sciences 42 (2019) 1–6.

[3] S.-E. Qian, Hyperspectral satellites, evolution, and development history, IEEE Journal of Selected Topics in Applied Earth Observations and Remote Sensing 14 (2021) 7032–7056.

[4] H. M. Dierssen, S. G. Ackleson, K. E. Joyce, E. L. Hestir, A. Castagna, S. Lavender, M. A. McManus, Living up to the hype of hyperspectral aquatic remote sensing: Science, resources and outlook, Frontiers in Environmental Science Volume 9 - 2021 (2021). doi:10.3389/fenvs.2021.649528.

[5] A. Tsokas, M. Rysz, P. M. Pardalos, K. Dipple, Sar data applications in earth observation: An overview, Expert Systems with Applications 205 (2022) 117342.

[6] H. Jin, G. Mountrakis, Fusion of optical, radar and waveform lidar observations for land cover classification, ISPRS Journal of Photogrammetry and Remote Sensing 187 (2022) 171–190.

[7] P. K. Sinha, A. Dutta, Multi-satellite task allocation algorithm for earth observation, in: 2016 IEEE Region 10 Conference (TENCON), IEEE, 2016, pp. 403–408.

[8] S. Huang, C. Colombo, F. Bernelli-Zazzera, Multi-criteria design of continuous global coverage walker and street-of-coverage constellations through property assessment, Acta Astronautica 188 (2021) 151–170.

[9] B. I. Society, Journal of the British Interplanetary Society, Vol. 34, The Society, 1934.

[10] C. Circi, E. Ortore, F. Bunkheila, Satellite constellations in sliding ground track orbits, Aerospace Science and Technology 39 (2014) 395–402.

[11] E. Ortore, M. Cinelli, C. Circi, A ground track-based approach to design satellite constellations, Aerospace Science and Technology 69 (2017) 458–464.

[12] F. Yao, J. Li, Y. Chen, X. Chu, B. Zhao, Task allocation strategies for cooperative task planning of multi-autonomous satellite constellation, Advances in space research 63 (2) (2019) 1073–1084.

[13] X. Wang, G. Wu, L. Xing, W. Pedrycz, Agile earth observation satellite scheduling over 20 years: Formulations, methods, and future directions, IEEE Systems Journal 15 (3) (2020) 3881–3892.

[14] Z. Chang, A. P. Punnen, Z. Zhou, Multi-strip observation scheduling problem for active-imaging agile earth observation satellites, Neural Computing and Applications (2023) 1–20.

[15] F. Bunkheila, E. Ortore, C. Circi, A new algorithm for agile satellite-based acquisition operations, Acta Astronautica 123 (2016) 121–128.

[16] M. Lemaître, G. Verfaillie, F. Jouhaud, J.-M. Lachiver, N. Bataille, Selecting and scheduling observations of agile satellites, Aerospace Science and Technology 6 (5) (2002) 367–381.

[17] S. Wang, L. Zhao, J. Cheng, J. Zhou, Y. Wang, Task scheduling and attitude planning for agile earth observation satellite with intensive tasks, Aerospace Science and Technology 90 (2019) 23–33.

[18] F. Yao, J. Li, B. Bai, R. He, Earth observation satellites scheduling based on decomposition optimization algorithm, International Journal of Image, Graphics and Signal Processing 2 (1) (2010) 10.

[19] G. Notomista, S. Mayya, Y. Emam, C. Kroninger, A. Bohannon, S. Hutchinson, M. Egerstedt, A resilient and energy-aware task allocation framework for heterogeneous multirobot systems, IEEE Trans. Robot. 38 (1) (2021) 159–179.

[20] G. Notomista, S. Mayya, S. Hutchinson, M. Egerstedt, An optimal task allocation strategy for heterogeneous multi-robot systems, in: Proc. 18th Eur. Control Conf., IEEE, 2019, pp. 2071–2076.

[21] L. Govoni, A. Cristofaro, A fault-tolerant task allocation framework for over-actuated multi-robot systems, in: IEEE 9th Int. Conf. Control Decis. Inf. Technol., 2023, pp. 287–292.

[22] R. Penrose, A generalized inverse for matrices, in: Math Proc. Cambridge Philos. Soc., Vol. 51, 1955, pp. 406–413.

[23] A. Khamis, A. Hussein, A. Elmogy, Multi-robot task allocation: A review of the state-of-the-art, Coop. robots and sensor networks (2015) 31–51.

[24] M. E. Grøtte, R. Birkeland, E. Honoré-Livermore, S. Bakken, J. L. Garrett, E. F. Prentice, F. Sigernes, M. Orlandić, J. T. Gravdahl, T. A. Johansen, Ocean color hyperspectral remote sensing with high resolution and low latency—the hypso-1 cubesat mission, IEEE Trans. Geosci. Remote Sens. 60 (2021) 1–19.

[25] S. Berg, S. Bakken, R. Birkeland, C. Chiatante, J. L. Garrett, T. A. Johansen, Ground systems software for automatic operation of the HYPSO-2 hyperspectral imaging satellite, in: Sensors, Systems, and Next-Generation Satellites XXVII, Vol. 12729, SPIE, 2023, pp. 277–286.

[26] B. Rhodes, Skyfield: Generate high precision research-grade positions for stars, planets, moons, and earth satellites, Astrophysics Source Code Library.
URL `https://ui.adsabs.harvard.edu/abs/2019ascl.soft07024R`

[27] E. F. Prentice, M. E. Grøtte, F. Sigernes, T. A. Johansen, Design of a hyperspectral imager using cots optics for small satellite applications, in: International Conference on Space Optics — ICSO 2020, Vol. 11852, SPIE, 2021, p. 1185258.
URL https://doi.org/10.1117/12.2599937

[28] N. Lazreg, R. Bouchiha, K. Besbes, Registration and correction techniques in cubesat remote sensing images, in: 2017 International Conference on Engineering & MIS (ICEMIS), IEEE, 2017, pp. 1–7.

[29] A. Bemporad, M. Morari, Control of systems integrating logic, dynamics, and constraints, Automatica 35 (3) (1999) 407–427.

[30] S. Katoch, S. S. Chauhan, V. Kumar, A review on genetic algorithm: past, present, and future, Multimedia tools and applications 80 (2021) 8091–8126.

[31] Gurobi Optimization LLC, Gurobi optimizer, https://www.gurobi.com (2021).